MODIS Polarization-Sensitivity Analysis

Jun-Qiang Sun and Xiaoxiong Xiong

***Abstract*—The Moderate Resolution Imaging Spectroradiometer (MODIS) is one of the primary instruments in the Earth Observing System (EOS). Currently, MODIS instruments are onboard the NASA EOS Terra and Aqua spacecraft launched in December 1999 and May 2002, respectively. The MODIS reflective solar bands (RSBs) are sensitive to the polarization of incident light, particularly for the visible bands. To derive accurate top-of-the-atmosphere radiances, it is essential to know the polarization sensitivity, characterized by a polarization factor and phase angle, of the instruments. From prelaunch polarization sensitivity measurements, the polarization factors and phase angles for all visible and near-infrared bands of both instruments are derived, analyzed, and compared. The polarization factors are wavelength, angle of incidence on the MODIS scan mirror, and detector-dependent. For Terra MODIS, they are also mirror-side-dependent. The 412-nm band has the largest polarization factor, which is about 0.04 for both instruments. The polarization factors of all other bands are either smaller than or close to 0.02, which is the polarization requirement for the MODIS RSB whose wavelengths are longer than 412 nm. The unexpected one-, three-, and four-cycle anomalies observed in the measurements are analyzed. These anomalies are shown to be likely due to the nonuniformity of the light source and the retro-reflected light from the MODIS optical system. Their impacts on the derived polarization parameters are estimated and discussed.**

***Index Terms*—Moderate Resolution Imaging Spectroradiometer (MODIS), polarization, reflective solar bands (RSBs).**

I. Introduction

THE MODERATE Resolution Imaging Spectroradiometer (MODIS) is a cross-track scanning radiometer [1]–[3]. Currently, MODIS instruments are operated onboard the Terra spacecraft, launched on December 18, 1999, and the Aqua spacecraft, launched on May 4, 2002 [4]. MODIS has 36 spectral bands, of which 20 are the reflective solar bands (RSBs) covering the wavelength range from 0.4–2.1 μm. MODIS views the entire Earth surface approximately daily via a two-side scan mirror that provides a swath of 2330 km cross track by 10 km along track (at nadir) each scan. It monitors the Earth–atmosphere system through visible and infrared measurements. MODIS data are used to study the oceans, atmosphere, and land [5]–[8].

The RSB are calibrated on-orbit through the use of an onboard solar-diffuser (SD) panel (made of Spectralon), the Moon, and an onboard spectroradiometric calibration assembly [9]–[13]. The light used in these calibrations is unpolarized, while the sunlight reflected from the Earth–atmosphere system may be strongly polarized [14], [15]. Since the MODIS RSBs are sensitive to the polarization of the incident light [16], the calibration coefficients derived from the calibrations using the unpolarized light may not be accurate for polarized incident light. The polarization specification is 0.02 for all MODIS RSBs except band 8, which has the shortest wavelength, 412 nm, among all MODIS bands. The polarization effect for band 8 was expected to be much stronger compared to other RSBs, and hence, no specification was designed. Considering that the calibration specification of the MODIS RSBs is 2% in reflectance, it is essential to know the polarization sensitivity of the instrument and correct the effect in the measured top-of-atmosphere radiances [17], [18].

MODIS polarization sensitivity was measured by Santa Barbara Remote Sensing (SBRS) using a polarization source assembly (PSA) as a source of polarized light [19]. The data were analyzed by both the SBRS and the MODIS Characterization Support Team at NASA/GSFC [16], [20]. A ray-tracing model has also been developed to simulate the MODIS polarization properties [21]. The measured data show that there are unexpected one-, three-, and four-cycle features in addition to the expected two-cycle variation when the plane of polarization rotates through 360°. The four-cycle anomaly is primarily due to the retro-reflectance of the focal-plane assemblies (FPAs) [16], [22]. In this paper, it is demonstrated that the one- and three-cycle anomalies are likely induced by the nonuniformity of the light source. It is also shown that the four-cycle anomaly is very sensitive to the filter used in the measurements. In Section II, we give a brief theoretical description of MODIS polarization analysis. In Section III, we analyze the data and derive the polarization parameters. We also analyze and discuss the impact of the nonuniformity of the light source and the retro-reflectance of the MODIS optical elements on the derived parameters. In Section IV, we analyze the derived parameters and compare the polarization performance of the two instruments on Terra and Aqua.

II. Theory

A. Polarization Formulism

Let $\mathbf{E}_s$ and $\mathbf{E}_p$ be two electric-field components of light incident on an optical element in directions $\mathbf{s}$ and $\mathbf{p}$ which are perpendicular to each other and form a right-handed local coordinate system with light traveling along vector $\mathbf{k}$ as described in Fig. 1. The vector $\mathbf{s}$ is perpendicular to the plane of incidence. Then, the Jones vector for incident light can be expressed as [23]

$$\mathbf{E} = \begin{pmatrix} E_s \\ E_p \end{pmatrix} \tag{1}$$

Manuscript received December 8, 2006; revised April 13, 2007.

J.-Q. Sun is with Science Systems and Applications, Inc., Lanham, MD 20706 USA.

X. Xiong is with the NASA Goddard Space Flight Center, Greenbelt, MD 20771 USA.

Digital Object Identifier 10.1109/TGRS.2007.900672

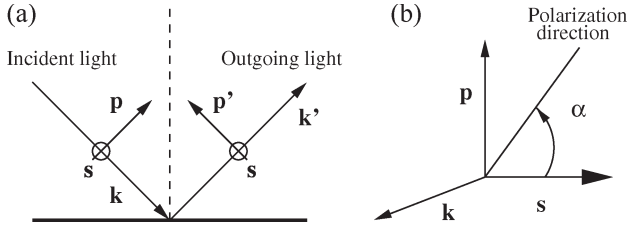

Fig. 1. Local coordinate system and polarization angle.

and the intensity of the light can be written as

$$I = \mathbf{E}^{\dagger}\mathbf{E} \tag{2}$$

where $\mathbf{E}^{\dagger}$ is the conjugate transpose of $\mathbf{E}$. We can also define a local coordinate system for outgoing light using outgoing traveling direction $\mathbf{k}'$, $\mathbf{s}' = \mathbf{s}$, and $\mathbf{p}' = \mathbf{k}' \times \mathbf{s}$, as shown in Fig. 1, and express the outgoing light in the coordinate system as

$$\mathbf{E}' = \begin{pmatrix} E_{s'} \\ E_{p'} \end{pmatrix}. \tag{3}$$

The components of the incident and outgoing light on reflection or refraction can be connected by a 2-D Jones matrix $\mathbf{u}$, given by

$$\mathbf{E}' = \mathbf{u}\mathbf{E}. \tag{4}$$

The matrix is determined by the optical property of the surface and could be complex.

For any optical instrument, there are usually several mirrors, lens, filters, and other elements along the optical path from the incident port to the detectors on its focal planes. However, we can still connect the incident light and the light that finally reaches the detectors by a 2-D Jones matrix, i.e.,

$$\mathbf{E}' = \mathbf{U}\mathbf{E} \tag{5}$$

where $\mathbf{U}$ is a product of Jones matrices of all individual elements and the matrices, which transform the vector from the outgoing local coordinate system of the previous element to the incident local coordinate system of the next element, in a sequential order. The intensity of the light reaching the detectors on the instrument's focal planes is given by

$$I' = \mathbf{E}^{\dagger}\mathbf{M}\mathbf{E} \tag{6}$$

where

$$\mathbf{M} = \mathbf{U}^{\dagger}\mathbf{U} \tag{7}$$

is a 2-D Hermitian matrix. For linear polarized light, (1) becomes

$$\mathbf{E} = \begin{pmatrix} \cos(\alpha) \\ \sin(\alpha) \end{pmatrix} E \tag{8}$$

where E is the amplitude of the electric vector, α is the angle between the direction of the electronic field, and vector $\mathbf{s}$ in the local coordinate system, as shown in Fig. 1. Substituting (8) into (6), we can get

$$I' = hI\left\{1 + a\cos\left[2\left(\alpha + \delta\right)\right]\right\} \tag{9}$$

according to Appendix A, where h, a, and δ are transmittance, polarization factor, and polarization phase angle, respectively, of the optical system. With a constant intensity of the incident light, the power, finally reaching the detectors on the focal plane of the instrument, varies with the polarization angle, and a is the relative amplitude of this change.

For a light with random phase and electric-field direction in the plane perpendicular to the traveling direction, we can write

$$I' = hI\int D(\alpha)\left\{1 + a\cos\left[2\left(\alpha + \delta\right)\right]\right\} d\alpha \tag{10}$$

where $D(\alpha)$ is the probability of the light's electric field vibrating along the direction described by polarization angle α. When $D(\alpha)$ is a constant, the light is unpolarized, such as sunlight. When $D(\alpha)$ is not a constant, we can always find the direction along which $D(\alpha)$ has a maximum value. The symbol μ is used to denote the angle between this direction and the vector $\mathbf{s}$ in the local coordinate formed by vectors $\mathbf{s}$, $\mathbf{p}$, and $\mathbf{k}$, as described in Fig. 1. Let us assume that $D(\alpha)$ is symmetric with respect to the maximum direction. Replacing α by $\alpha' + \mu$, (10) becomes

$$\begin{aligned} I' &= hI\int D(\alpha' + \mu)\left\{1 + a\cos\left[2\left(\alpha' + \mu + \delta\right)\right]\right\} d\alpha' \\ &= hI\int D(\alpha' + \mu)\left\{1 + a\cos\left(2\alpha'\right)\cos\left[2\left(\mu + \delta\right)\right]\right. \\ &\qquad \left. - a\sin\left(2\alpha'\right)\sin\left[2\left(\mu + \delta\right)\right]\right\} d\alpha' \\ &= hI\int D(\alpha' + \mu)\left\{1 + a\cos\left(2\alpha'\right)\cos\left[2\left(\mu + \delta\right)\right]\right\} d\alpha' \\ &= h\left\{I + a(I_1 - I_2)\cos\left[2\left(\mu + \delta\right)\right]\right\} \end{aligned} \tag{11}$$

where

$$I_1 = I\int D(\alpha' + \mu)\cos^2(\alpha')d\alpha' \tag{12}$$

$$I_2 = I\int D(\alpha' + \mu)\sin^2(\alpha')d\alpha' \tag{13}$$

are the total intensity of the light projected in the maximum direction and that in the direction perpendicular to the maximum direction, respectively. If we define

$$f = \frac{I_1 - I_2}{I} \tag{14}$$

which measures the polarization of the incident light and is, hereafter, referred to as the scene polarization factor, (11) can

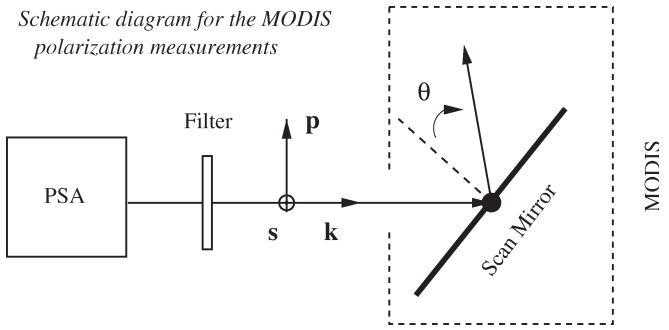

Fig. 2. Schematic diagram for MODIS polarization-sensitivity measurements.

be further rewritten as

$$I' = hI\left\{1 + fa\cos\left[2(\mu+\delta)\right]\right\}. \tag{15}$$

B. MODIS Polarization-Analysis Algorithms

Both Terra and Aqua MODIS polarization-sensitivity measurements were made with a PSA at SBRS [15]. The PSA provides a full-aperture polarized source to MODIS. By rotating the Ahrens polarizer prism, the polarization direction varies from 0° to 360°. Fig. 2 is a schematic diagram of the measurement. Let $\mathbf{E}_{\rm PSA}$ be the polarized light produced by the PSA. In the local coordinate system of the MODIS scan mirror, $\mathbf{E}_{\rm PSA}$ can be expressed as

$$\mathbf{E}_{\rm PSA} = E_{\rm PSA}(\alpha)\begin{pmatrix}\cos(\alpha)\\ \sin(\alpha)\end{pmatrix} \tag{16}$$

where α is the angle between the polarization direction and the vector $\mathbf{s}$, which is approximately along the rotation axis of the scan mirror, and $E_{\rm PSA}(\alpha)$ is the magnitude of $\mathbf{E}_{\rm PSA}$, which may vary with the polarization direction due to the nonuniformity of the Ahrens polarizer prism and spatial nonuniformity of the light source or other reasons.

From the data collected for both Terra and Aqua MODIS polarization sensitivity characterization, an unexpected so-called four-cycle anomaly has been found in near-infrared (NIR) bands. The anomaly was explained as the multiple passes between the PSA and the MODIS focal-plane filters [16], [22]. In the next section, it will be shown that the anomaly also depends on the filter placed between the PSA and the scan mirror of the MODIS.

Let $\mathbf{E}_{\rm refl}$ be the retro-reflected light, reflected by any surface of any optical elements including the focal planes in the optical path and then reflected by the prism. We can always connect $\mathbf{E}_{\rm refl}$ and $\mathbf{E}_{\rm PSA}$ by a Jones matrix $\mathbf{V}$, which is a function of the optical parameters of the Ahrens prism, the filter, the optical elements in between, and distances among all the involved elements, such that

$$\mathbf{E}_{\rm refl} = \mathbf{V}\mathbf{E}_{\rm PSA}. \tag{17}$$

Since only the component along the direction of $\mathbf{E}_{\rm PSA}$ can pass through the Ahrens polarizer prism, the light which is reflected by the focal planes (or other optical elements) and finally becomes part of the output of the polarizer is

$$\begin{aligned}\mathbf{E_1} &= \begin{pmatrix}\cos(\alpha)\\ \sin(\alpha)\end{pmatrix}\mathbf{E}_{\rm refl}\begin{pmatrix}\cos(\alpha)\\ \sin(\alpha)\end{pmatrix}\\ &= (\cos(\alpha)\ \ \sin(\alpha))\,\mathbf{V}\begin{pmatrix}\cos(\alpha)\\ \sin(\alpha)\end{pmatrix}\mathbf{E}_{\rm PSA}.\end{aligned} \tag{18}$$

Assuming that the light reflected by the focal planes (or other optical elements) more than once is negligible, the total incident light on the MODIS scan mirror can be expressed as

$$\mathbf{E} = \left[1 + (\cos(\alpha)\ \ \sin(\alpha))\,\mathbf{V}\begin{pmatrix}\cos(\alpha)\\ \sin(\alpha)\end{pmatrix}\right]\mathbf{E}_{\rm PSA}. \tag{19}$$

Substituting (19) into (6), the light intensity reaching a detector on the MODIS focal planes can be expressed as

$$\begin{aligned}I'(\alpha) &= w(\alpha)\mathbf{E}^{\dagger}_{\rm PSA}\mathbf{M}\mathbf{E}_{\rm PSA}\\ &= hI_{\rm PSA}(\alpha)w(\alpha)\left\{1 + a\cos\left[2(\alpha+\delta)\right]\right\}\end{aligned} \tag{20}$$

where use has been made of (9)

$$I_{\rm PSA}(\alpha) = E^{*}_{\rm PSA}(\alpha)E_{\rm PSA}(\alpha) \tag{21}$$

$$w(\alpha) = \left[1 + (\cos(\alpha)\sin(\alpha))\,V\begin{pmatrix}\cos(\alpha)\\ \sin(\alpha)\end{pmatrix}\right]^2. \tag{22}$$

According to Appendix B, $w(\alpha)$ can be rewritten as

$$w(\alpha) = b_0\left\{1 + b_1\cos\left[2(\alpha+\tau_1)\right] + b_2\cos\left[4(\alpha+\tau_2)\right]\right\} \tag{23}$$

where b_0, b_1, τ_1, b_2, and τ_2 are functions of the optical properties of the elements involved in the production of $\mathbf{E}_{\rm refl}$.

From (20) and (23), we have

$$I'(\alpha) = I'(\pi+\alpha) \tag{24}$$

if $I_{\rm PSA}(\alpha)$ does not vary with polarization direction. However, the measured MODIS response to the polarized light shows that this is not always the case. In fact, a one-cycle oscillation has been clearly observed in both Aqua and Terra MODIS polarization-sensitivity measurements. In the next section, it is shown that a three-cycle oscillation is also observed in the measurements. As aforementioned, this might be induced by the nonuniformity of the polarizer prism or other mechanical reasons.

We can always express $I_{\rm PSA}(\alpha)$ as Fourier series

$$I_{\rm PSA}(\alpha) = I_{\rm PSA}\left\{1 + \sum_i c_i\cos\left[i(\alpha+\sigma_i)\right]\right\} \tag{25}$$

where $I_{\rm PSA}$ is the averaged value of $I_{\rm PSA}(\alpha)$ and c_i and σ_i are parameters of the PSA and the experimental setup. Then,

TABLE I
MODIS VIS AND NIR BANDS

Band	Number of Detectors	Spatial Resolution	Center Wavelength (nm)	Bandwith (nm)	FPA
1	40	250m	645	50	NIR
2	40	250m	858	35	NIR
3	20	500m	469	20	VIS
4	20	500m	555	20	VIS
8	10	1km	412	15	VIS
9	10	1km	443	10	VIS
10	10	1km	488	10	VIS
11	10	1km	531	10	VIS
12	10	1km	551	10	VIS
13	10	1km	667	10	NIR
14	10	1km	678	10	NIR
15	10	1km	748	10	NIR
16	10	1km	869	15	NIR
17	10	1km	905	30	NIR
18	10	1km	936	10	NIR
19	10	1km	940	50	NIR

substituting (23) and (25) into (20), we get

$$I'(\alpha) = hb_0 I_{\mathrm{PSA}} \left\{ 1 + \sum_i c_i \cos\left[i(\alpha + \sigma_i)\right] \right\} \times \left\{1 + b_1 \cos\left[2(\alpha + \tau_1)\right] + b_2 \cos\left[4(\alpha + \tau_2)\right]\right\} \times \left\{1 + a \cos\left[2(\alpha + \delta)\right]\right\}. \quad (26)$$

Table I lists the wavelengths and other specified information of all MODIS visible (VIS) and NIR bands. Since optical properties of an optical system are wavelength-dependent, all the parameters in (26) are band-dependent. The detectors of each band are distributed on an array along the track direction. The optical paths of these detectors are slightly different. Thus, the parameters in (26) are also detector-dependent. In addition, they are functions of the mirror side and angle of incidence (AOI), on which the reflectance of the scan mirror depends. Therefore, the at-detector signal can be written as

$$S^{BDM\theta}(\alpha) = G^{BDM\theta} I^B_{\mathrm{PSA}} \left\{ 1 + \sum_{i>0} c_i^{BDM\theta} \cos\left[i\left(\alpha + \sigma_i^{BDM\theta}\right)\right] \right\} \times \left\{1 + b_1^{BDM\theta} \cos\left[2\left(\alpha + \tau_1^{BDM\theta}\right)\right] + b_2^{BDM\theta} \cos\left[4\left(\alpha + \tau_2^{BDM\theta}\right)\right]\right\} \times \left\{1 + a^{BDM\theta} \cos\left[2\left(\alpha + \delta^{BDM\theta}\right)\right]\right\} \quad (27)$$

where B is the band number, D is the detector number, M is the scan-mirror side, θ is the scan-mirror AOI, I^B_{PSA} is the light intensity at the wavelength of band B, and $G^{BDM\theta}$ is the gain of the detector D of band B with mirror-side M at AOI of θ. Equation (27) will be used to fit the data of the MODIS polarization-sensitivity measurements.

When (27) is applied to fit the measured MODIS responses to the polarized light, we can only get one set of amplitude and phase angle for the two-cycle oscillation. We cannot determine each individual contribution of the polarization effect, the nonuniformity of the light source, and the retro-reflected light to the two-cycle oscillation. The fitted amplitude and phase angle is the total effect of the three sources. From (27), it is seen that the odd-cycle oscillations can only come from the nonuniformity of the light source. Thus, $c_1^{BDM\theta}$ and $c_3^{BDM\theta}$ can be determined from the measured responses. With them, we can estimate $c_2^{BDM\theta}$ and, then, the uncertainty of the fitted polarization factor $a^{BDM\theta}$ due to the nonuniformity of the light source. We can also determine $b_2^{BDM\theta}$ with an approximation that $c_4^{BDM\theta}$ is negligible from the four-cycle oscillation of the measured responses. Similarly, we can estimate $b_1^{BDM\theta}$ from $b_2^{BDM\theta}$ and, then, the uncertainty of the fitted-polarization factor $a^{BDM\theta}$ due to the retro-reflected light.

C. Polarization Correction to MODIS Earth-View (EV) Reflectance and Radiance

The MODIS RSB primary product is the EV reflectance

$$\rho_{\mathrm{EV}} \cos(\theta_{\mathrm{EV}}) = m_1 dn^*_{\mathrm{EV}} d^2_{E-S} \quad (28)$$

where ρ_{EV} is the Earth-scene bidirectional-reflectance factor, θ_{EV} is the solar-illumination angle of the Earth scene, dn^*_{EV} is the Earth-scene digital response with correction for background signal, instrumental temperature effect, and sensor response versus scan angle, $d_{\mathrm{E-S}}$ is the Earth–Sun distance at the time of the measurement in units of AU, and m_1 is a calibration-scaling factor determined on orbit using the onboard SD [5].

The SD is considered to provide a nonpolarized light source for MODIS RSB calibration. Thus, (28) is valid only when the EV light is nonpolarized. According to (15), (28) should be modified and rewritten as

$$\rho_{\mathrm{EV}} \cos(\theta_{\mathrm{EV}}) = \frac{\left[\rho_{\mathrm{EV}} \cos(\theta_{\mathrm{EV}})\right]_{L1B}}{c_{\mathrm{pl}}(B, D, M, \theta)} \quad (29)$$

where

$$c_{\mathrm{pl}}(B, D, M, \theta) = 1 + a^{BDM\theta} f \cos\left[2(\mu + \delta^{BDM\theta})\right] \quad (30)$$

is the polarization-correction factor, and $[\rho_{\mathrm{EV}} \cos(\theta_{\mathrm{EV}})]_{L1B}$ is the MODIS L1B EV reflectance. The scene polarization factor f and the polarization angle μ depend on the wavelength of the band and vary with geolocation and the observation geometry.

III. MODIS POLARIZATION-SENSITIVITY ANALYSIS

A. Data Sets and Selection

Terra and Aqua MODIS polarization sensitivities were measured by SBRS. The measurements were done at five scan angles ($-45^\circ, -22.5^\circ, 0^\circ, 22.5^\circ$, and 45°) for both instruments, 25 polarization angles ($-180^\circ, -165^\circ, -150^\circ, -135^\circ, -120^\circ, -105^\circ, -90^\circ, -75^\circ, -60^\circ, -45^\circ, -30^\circ, -15^\circ, 0^\circ, 15^\circ, 30^\circ, 45^\circ, 60^\circ, 75^\circ$, $90^\circ, 105^\circ, 120^\circ, 135^\circ, 150^\circ, 165^\circ$, and 180°) for Aqua, and 13 polarization angles ($180^\circ, -150^\circ$, $-120^\circ, -90^\circ, -60^\circ, -30^\circ, 0^\circ, 30^\circ, 60^\circ, 90^\circ, 120^\circ, 150^\circ$, and 180°) for Terra. The scan angle ω of the MODIS EV varies from -55° to 55° and is related to the AOI of the scan mirror θ by

$$\theta = (\omega + 76^\circ)/2. \quad (31)$$

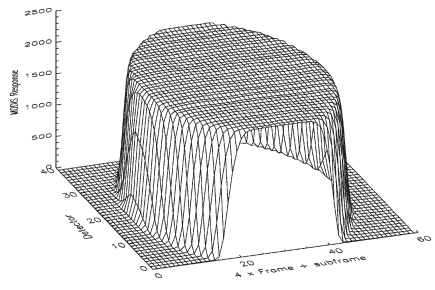

Fig. 3. Aqua band 1 response to PSA light in one scan.

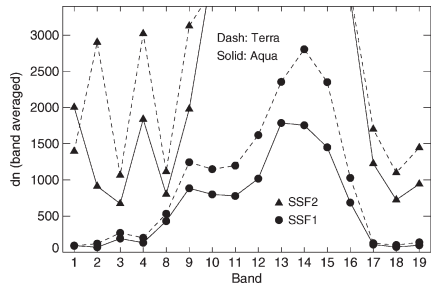

Fig. 4. MODIS band-averaged polarization response (dn). For the data measured with filter SSF2, bands 10–16 are saturated.

Fig. 3 illustrates the response of the detectors of Aqua band 1 to the PSA light, which shows that the light source has a limited size. The MODIS frame (1-km sample) number F is related to the scan angle by

$$\omega = 110F/1353 - 55^\circ \tag{32}$$

where F starts from zero and ends at 1353. The data shown in Fig. 3 were measured at the scan angle of -45°. This means that the real frame number for the center of the image in Fig. 3 is 123 according to (32). The frame number in the plot is the relative frame number. From the image, it is seen that end detectors have fewer frames viewing the PSA light and may have larger uncertainties in the polarization parameters derived from these data. $S^{BDM\theta}(\alpha)$ is obtained by averaging over the response of the frames (1-km sample), which views the light source, subframes (250- or 500-m samples), and scans of mirror-side M.

During the MODIS polarization-sensitivity measurements, a neutral density filter was placed between the PSA and the scan mirror of the MODIS, as shown in Fig. 2. Two filters, SSF1 and SSF2, with different transmittances were alternatively used in the measurements. Fig. 4 shows the band-averaged response (averaged over detectors, subframes, mirror sides, frames, and polarization angles) for both instruments. The averaged response measured with filter SSF2 are much larger than those obtained with filter SSF1 as expected. The former are saturated for bands 10–16, while the latter are too small for bands 1–4 and 17–19. Thus, the data measured with filter SSF2 are applied to derive polarization parameters for bands 1–4, 8–9, and 17–19 while those observed with filter SSF1 are used for bands 10–16. The polarization parameters for bands 8 and 9 can also be derived from the data measured with SSF1, but the derived parameters should have larger uncertainties.

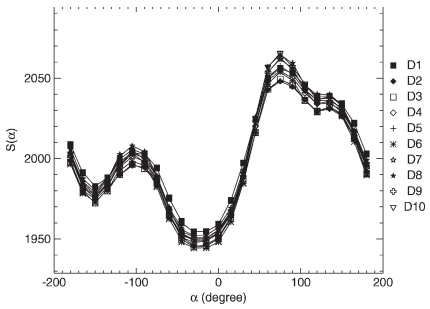

Fig. 5. Aqua MODIS band 1 dn versus polarization angle.

B. Nonuniformity of the Light Source

The $S^{BDM\theta}(\alpha)$ obtained from the data measured with SSF1 for Aqua band 1 mirror-side 1 at $\theta = 15.5^\circ$ (corresponding to scan angle of -45°) is shown in Fig. 5. A one-cycle oscillation is clearly seen in this plot. This one-cycle phenomenon is also observed in all other bands. The nonuniformity of the light provided by the PSA light can induce the one-cycle oscillation. They can also induce three-cycle phenomenon and may have contributions to the two- and four-cycle oscillation, which cannot be separated from those contributed by the polarization of the instrument and the retro-reflection of the optical system as aforementioned. From (27), we get

$$\begin{aligned}\frac{S^{BDM\theta}(\alpha)}{S^{BDM\theta}(\alpha+\pi)} &= \frac{1+\sum\limits_{i=1,3,\ldots} C_i^{BDM\theta}(\alpha)\Big/\left[1+\sum\limits_{i=2,4,\ldots} C_i^{BDM\theta}(\alpha)\right]}{1-\sum\limits_{i=1,3,\ldots} C_i^{BDM\theta}(\alpha)\Big/\left[1+\sum\limits_{i=2,4,\ldots} C_i^{BDM\theta}(\alpha)\right]} \\ &\approx \frac{1+\sum\limits_{i=1,3,\ldots} C_i^{BDM\theta}(\alpha)}{1-\sum\limits_{i=1,3,\ldots} C_i^{BDM\theta}(\alpha)}\end{aligned} \tag{33}$$

where

$$C_i^{BDM\theta}(\alpha) = c_i^{BDM\theta}\cos\left[i\left(\alpha+\sigma_i^{BDM\theta}\right)\right]. \tag{34}$$

The ratio defined in the left side of (33) is not sensitive to even-order oscillations and shows odd-cycle oscillations. Fig. 6 shows $S^{BDM\theta}(\alpha)/S^{BDM\theta}(\alpha+\pi)$ for Aqua band 1. It is clearly seen that there is a nonnegligible three-cycle oscillation besides the one-cycle oscillation. By fitting (33) to measured data with a least mean-square-fit approach, we can derive $c_1^{BDM\theta}$ and $c_3^{BDM\theta}$ for all bands, detectors, mirror sides, and the five AOIs of the scan mirror.

The derived one-cycle factor $c_1^{BDM\theta}$ and three-cycle factor $c_3^{BDM\theta}$ at $\omega = -45^\circ(\theta = 15.5^\circ)$ for the two instruments are shown in Figs. 7 and 8, respectively. The factors for other scan angles are also derived. The results show that these factors are scan-angle-independent. The one- and three-cycle oscillations cannot be produced by the polarization sensitivity of the instruments and the retro-reflected light, as shown in Section II. For Aqua, both $c_1^{BDM\theta}$ and $c_3^{BDM\theta}$ do not change much with band and detector except band 8. They are about

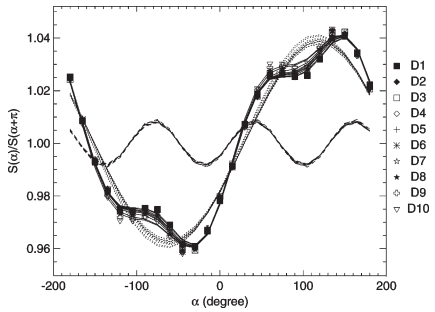

Fig. 6. Aqua MODIS band 1 dn ratio $S(\alpha)/S(\alpha+\pi)$: Symbols, measured ratio. Dotted lines, ratio with one-cycle oscillation only. Dashed lines, ratio with three-cycle oscillation only. Solid lines, ratio with both one- and three-cycle oscillations.

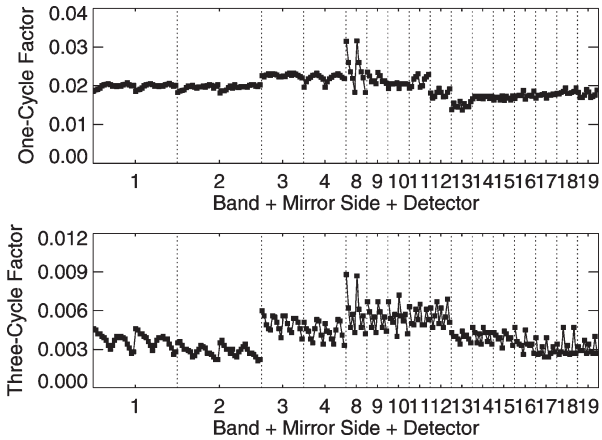

Fig. 7. Aqua one- and three-cycle oscillation factors. The numbers on the abscissa are MODIS band numbers. For each band, the first half of the data plotted is for all detectors on mirror-side one, and the second half of the data is for all detectors on mirror-side two.

0.02 and 0.005, respectively. With a simple linear assumption for the decay of $c_i^{BDM\theta}$ with index i, we can estimate $c_2^{BDM\theta}$ to be 0.012. $c_2^{BDM\theta}$ could be smaller or larger depending on the real nonuniformity of the light source. For Terra, both $c_1^{BDM\theta}$ and $c_3^{BDM\theta}$ are smaller as compared to Aqua and are spectral-dependent. Similarly, we can estimate the Terra factors $c_2^{BDM\theta}$ to be around 0.007 for bands 8–10, 0.004 for bands 1–4 and 10–13, and 0.002 for the other bands. Due to this, the nonuniformity of the light source may have an impact on the derived polarization parameters as large as 0.012 for all Aqua RSB and 0.007 for Terra bands 8–10, 0.004 for Terra bands 1–4 and 10–13, and 0.002 for other Terra RSB.

Having obtained $c_1^{BDM\theta}$ and $c_3^{BDM\theta}$, we define

$$y^{BDM\theta}(\alpha) = \frac{S^{BDM\theta}(\alpha)}{1 + \sum\limits_{i=1,3} c_i^{BDM\theta} \cos\left[i\left(\alpha + \sigma_i^{BDM\theta}\right)\right]}. \quad (35)$$

Fig. 9 shows the $y^{BDM\theta}(\alpha)$ obtained from the data measured with SSF1 for Aqua band 1. It can be seen from the plot that the one- and three-cycle oscillations have been removed, thereby leaving only the two- and four-cycle oscillations.

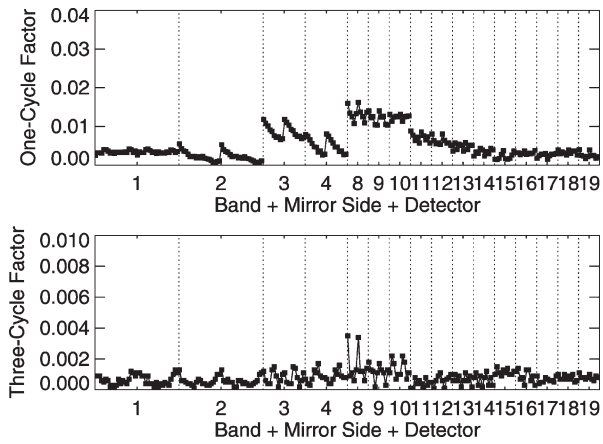

Fig. 8. Terra one- and three-cycle oscillation factors.

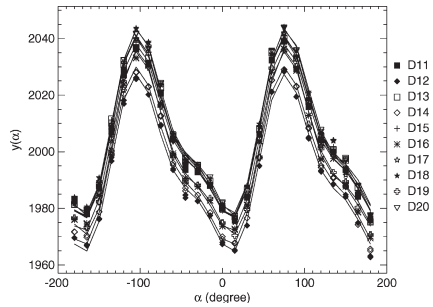

Fig. 9. Aqua MODIS band 1 dn with removal of one- and three-cycle oscillations. The measurements were done with filter SSF2.

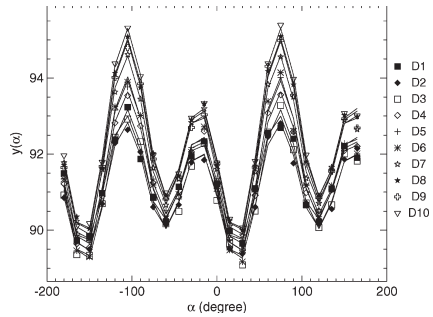

Fig. 10. Aqua MODIS band 1 dn with removal of one- and three-cycle oscillations. The measurements were done with filter SSF1.

C. Four-Cycle Effect

Fig. 10 shows the $y^{BDM\theta}(\alpha)$ obtained from the data measured with SSF2 for Aqua band 1 at $\theta = 15.5^\circ$. There is a strong four-cycle oscillation in the plot, which is believed to be caused by the retro-reflected light of the focal plane [16]. The four-cycle oscillation in Fig. 9 is not apparent while that in Fig. 10 has an amplitude half that of the amplitude of the two-cycle oscillation. The only difference in the two measurements is the filter, one with SSF1 while the other with SSF2. This indicates that the four-cycle oscillation depends not only on the retro-reflectance of the focal plane but also on the filter placed between the PSA and the scan mirror of MODIS.

The retro-reflected light may contribute to the two-cycle oscillation. However, we cannot separate its contribution from the polarization of the instrument [22]. We have to ignore the two-cycle oscillation term of the retro-reflected light when we

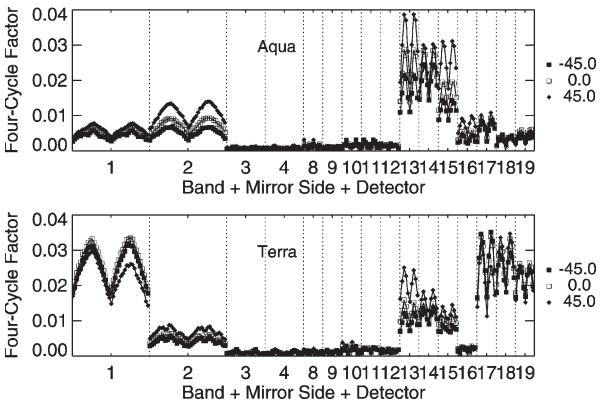

Fig. 11. Four-cycle oscillation factors for both Aqua and Terra.

fit (27) to the measured responses. Then, from (27) and (35), we can rewrite

$$y^{BDM\theta}(\alpha) = G^{BDM\theta} I^{B}_{\mathrm{PSA}} \left\{1 + b_2^{BDM\theta} \cos\left[4\left(\alpha + \tau_2^{BDM\theta}\right)\right]\right\} \times \left\{1 + a^{BDM\theta} \cos\left[2\left(\alpha + \delta^{BDM\theta}\right)\right]\right\}. \quad (36)$$

By fitting (36) to $y^{BDM\theta}(\alpha)$ obtained from (35) with least mean square fit, we can derive $b_2^{BDM\theta}$, $\tau_2^{BDM\theta}$, $a^{BDM\theta}$, and $\delta^{BDM\theta}$ for each set of B, D, M, and θ. From $b_2^{BDM\theta}$, we can estimate $b_1^{BDM\theta}$ and, then, the uncertainty of the fitted polarization factor $a^{BDM\theta}$ due to the retro-reflected light.

Fig. 11 shows the obtained $b_2^{BDM\theta}$ for Aqua and Terra MODIS RSB at $\omega = -45^\circ$, 0°, and 45°. For both instruments, the impact of the retro-reflected light on VIS bands is negligible. The remaining bands are NIR bands. Among them, bands 1–2 and 16–19 for Aqua and bands 2 and 16 for Terra have reasonably small impact (around 0.5%) due to the retro-reflectance. According to Waluschka [22], the contribution of the retro-reflectance to the two-cycle oscillation is much smaller than its effect on the four-cycle oscillation. Then, for bands 1–12 and 16–19 for Aqua and bands 2–12 and 16 for Terra, the impact of the retro-reflectance on their derived polarization parameters can be considered negligible. The retro-reflectance may bring nonnegligible contributions to the two-cycle oscillation for Aqua bands 13–15 and Terra bands 1, 13–15, and 17–19. Because of this, these bands may have larger uncertainties in their derived polarization parameters.

Fig. 12 compares the measured response of Aqua band 1 and the simulated response for the band with the fitted parameters. They match quite well. This is also true for all other bands. Thus, (27) well describes the MODIS polarization-sensitivity measurements.

IV. MODIS Polarization Parameters

A. Aqua

Fig. 13 shows the variations of the prelaunch measured (and uncorrected) polarization factors $a^{BDM\theta}$ with the scan angle for Aqua band 8. The results show the polarization factors to be detector- and AOI-dependent but independent of mirror side. The polarization factors are larger for larger AOI, which correspond to larger frame numbers. The band-averaged polarization factors for all MODIS VIS and NIR bands are

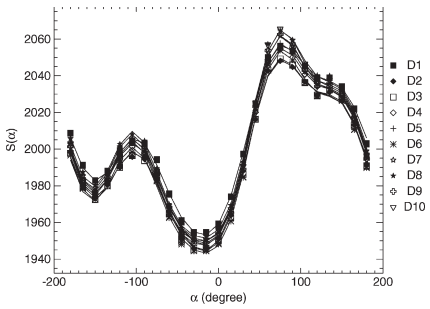

Fig. 12. Comparison among the measured response and those simulated with the fitted coefficients for Aqua band 1.

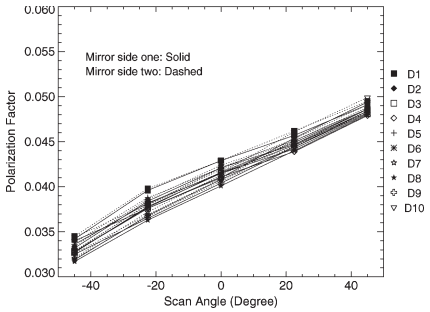

Fig. 13. Polarization factors for Aqua band 8.

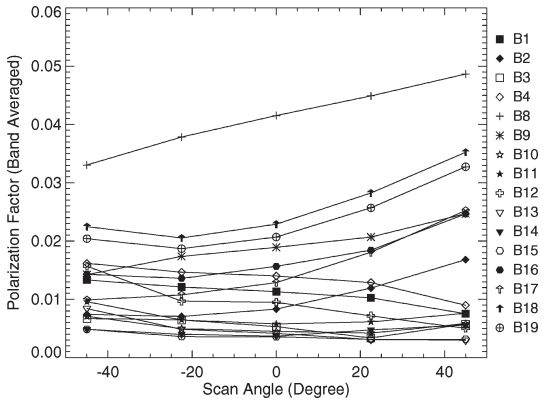

Fig. 14. Band-averaged polarization factors for Aqua RSB.

presented in Fig. 14. Among these bands, band 8 has the largest polarization factor. For most Aqua RSB, the polarization factors are smaller than the polarization specification, 0.02, except bands 18–19 at most AOI and bands 9, 16, and 17 at large AOI. Considering that the uncertainty of the polarization factors due to the nonuniformity of the light source is about 0.012, these bands may still satisfy the polarization specification.

Figs. 15 and 16 show the polarization factors and phase angles, respectively, for MODIS VIS and NIR bands at $\omega = -45^\circ$, 0°, and 45°. No obvious mirror-side dependence is observed in both parameters. This is consistent with the radiometric performance of the Aqua RSB both prelaunch and on-orbit. However, the parameters are detector-dependent, particularly for bands 2, 12, and 17–19. They vary continuously with the locations of the detectors on the FPA. For each band, the detectors are distributed along the track direction with the optical path of the center detector most close to the optical axis of the instrument. Thus, the optical paths are slightly detector-dependent. For

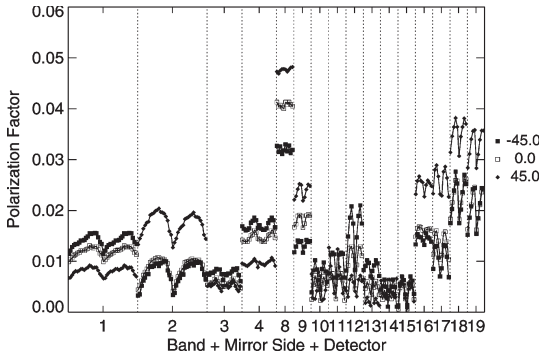

Fig. 15. Polarization factors for Aqua RSB.

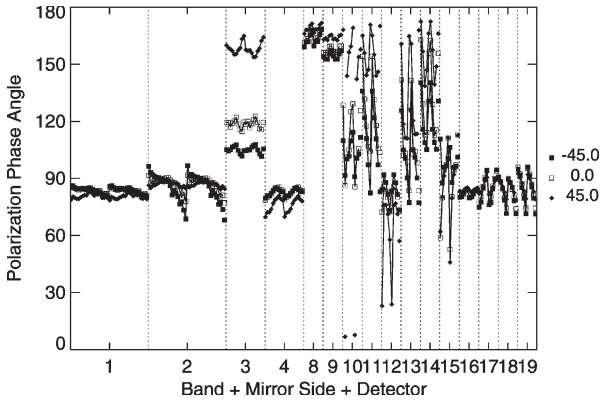

Fig. 16. Polarization phase angles for Aqua RSB.

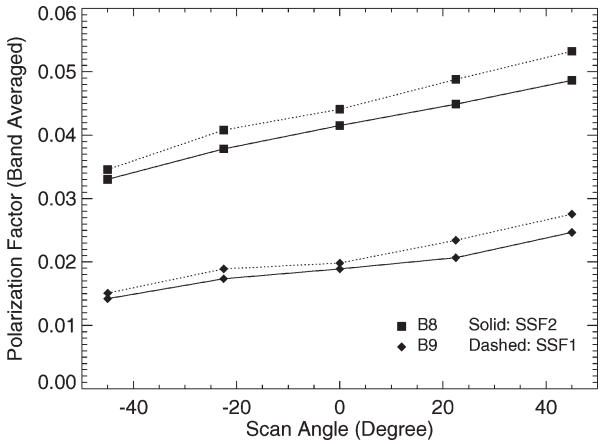

Fig. 17. Band-averaged polarization factors for Aqua bands 8 and 9. Solid lines are the factors derived from the measurements with filter SSF2 while dashed lines are those done from the measurements with filter SSF1.

most bands, the polarization factors of the center detectors are larger while those of edge detectors are smaller, particularly for bands 2 and 17.

Fig. 17 shows the band-averaged polarization factors for bands 8 and 9, which are derived from the measured data with filter SSF1 and SSF2, separately. The solid lines are the factors derived from the data measured with filter SSF2 while the dashed lines are done using filter SSF1. The differences between the corresponding solid and dashed lines show the uncertainties of the parameters derived from different measurements for these two bands. They are about 0.004 and 0.003 for bands 8 and 9, respectively.

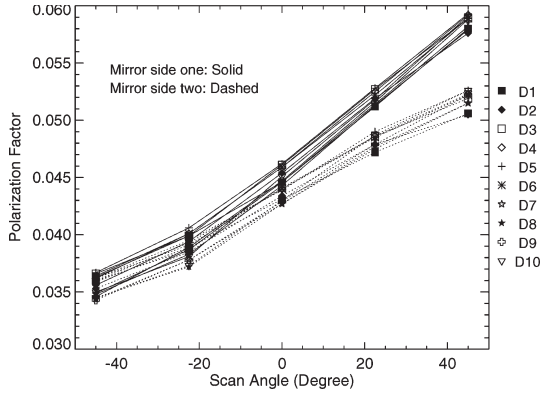

Fig. 18. Polarization factors for Terra band 8.

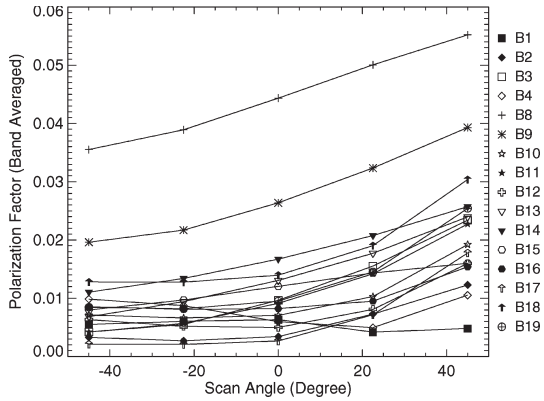

Fig. 19. Band-averaged polarization factors for Terra RSB.

B. Terra

Fig. 18 shows the variations of the polarization factors $a^{BDM\theta}$ of Terra band 8 detectors with the scan angle. As with the Aqua band 8 polarization factors shown in Fig. 15, the Terra band 8 polarization factors depend on both detectors and the AOI and are larger for larger AOIs. Unlike Aqua band 8, Terra band 8 polarization factors are mirror-side-dependent. The differences between the factors of the two mirror sides are small at small AOI but increase with AOI. Fig. 19 shows the band-averaged polarization factors for MODIS VIS and NIR bands. Band 8 has the largest polarization factor among both Terra and Aqua MODIS RSB. For most Terra RSB, the polarization factors are smaller than the polarization specification except band 9 and a few other bands at large AOIs.

Figs. 20 and 21 show the polarization factors and phase angles, respectively, for Terra MODIS VIS and NIR bands at $\omega = -45^\circ$, 0°, and 45°. The mirror-side and detector dependence is evident. The polarization factors for Terra change continuously with the location of the detectors on their FPA. This result is consistent with the one seen for Aqua. The polarization factors for center detectors are not always larger than those for edge detectors. Fig. 22 shows the band-averaged polarization factors for bands 8 and 9, which are derived from the measured data with filter SSF1 and SSF2, separately. The differences between the factors derived from the two sets of data are much smaller than those for Aqua. They are about 0.002 and 0.001 for bands B8 and B9, respectively. This indicates that the uncertainties

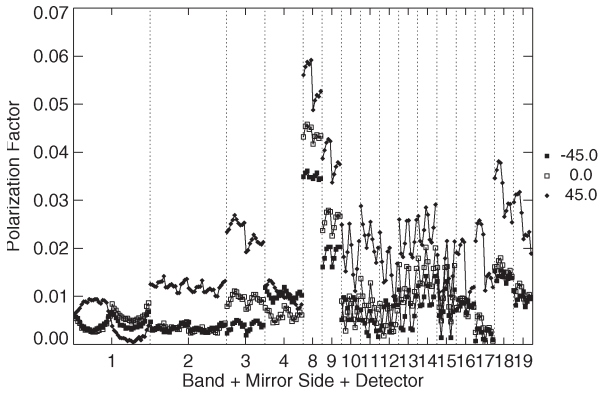

Fig. 20. Polarization factors for Terra RSB.

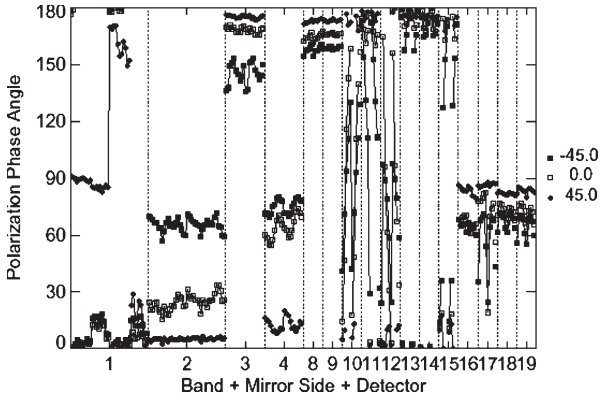

Fig. 21. Polarization phase angles for Terra RSB.

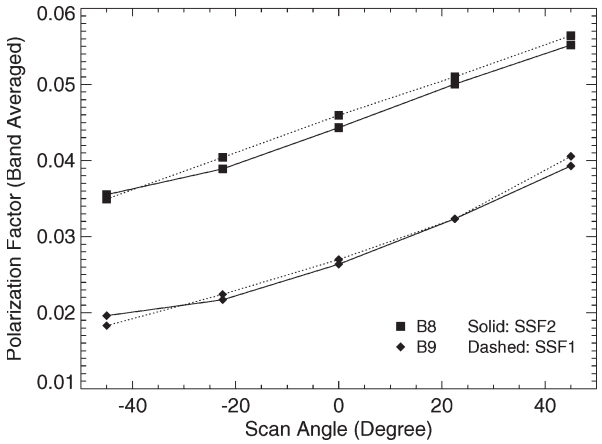

Fig. 22. Band-averaged polarization factors for Terra bands 8 and 9. Solid lines are the factors derived from the measurements with filter SSF2, while dashed lines are those done from the measurements with filter SSF1.

of the factors due to the light source are smaller for Terra than for Aqua.

C. Comparison and Discussion

Fig. 23 compares the polarization factors of the two instruments. They agree with each other reasonably well. The differences for VIS and NIR bands are about 0.005 and 0.01, respectively. For both instruments, the factors are largest for band 8, which has the shortest wavelength among all the bands.

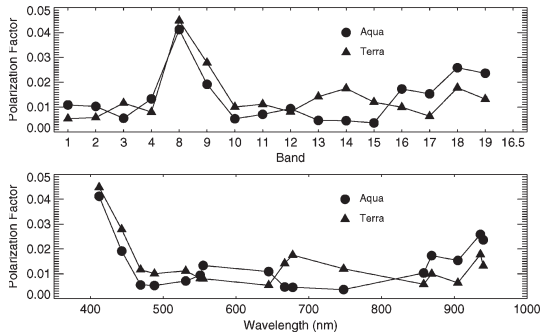

Fig. 23. Comparison between Aqua and Terra polarization factors.

They decrease with increasing wavelength through 412–469 nm and are relatively constant for bands with longer wavelength.

We have estimated the uncertainties in the derived polarization parameters due to the nonuniformity of the light source and retro-reflected light according to the derived amplitudes of the one-, three-, and four-cycle oscillations. The uncertainty in the derived polarization factors due to the nonuniformity of the light source is about 0.012 for all Terra RSB bands, 0.007 for Aqua bands 8–10, 0.004 for Aqua bands 1–4 and 10–13, and 0.002 for other Aqua bands. The uncertainty due to the retro-reflected light may have a significant impact on the quality of derived polarization parameters for the MODIS NIR bands. Considering the MODIS RSB uncertainty in reflectance is required to be less than 2% (desired to be much smaller for ocean bands), the nonuniformity of the light source should be reduced and the retro-reflected light should be controlled to a level so as have negligible contribution to the two-cycle oscillation. For future sensor-polarization characterization, the PSA needs to be improved to provide uniform light, and the measurement should be designed to avoid the retro-reflected light. If the nonuniformity of the light source cannot be greatly reduced, the variation of the light source with the polarization direction should be monitored. The measured variation of the light source with the polarization direction can be applied to determine the contribution of the nonuniformity of the light source to the two-cycle oscillation and, then, to distinguish the contribution from the polarization effect.

V. Conclusion

The polarization performance of both Aqua and Terra MODIS are analyzed using the prelaunch MODIS polarization-sensitivity measurements. Polarization factors and phase angles are derived for the VIS and NIR bands of both instruments. The derived polarization parameters are band-, AOI-, and detector-dependent. They are also mirror-side-dependent for Terra RSBs. The unexpected one-, three-, and four-cycle anomalies are analyzed, and their impacts on the derived parameters are discussed. For Aqua, the nonuniformity of the light source may bring an uncertainty to the derived polarization factors as large as 0.012. The retro-reflected light has also a nonnegligible impact on the derived polarization factors for several RSBs. The reduction of the nonuniformity of the light source and of the retro-reflected light is very important in characterization of a remote sensor's polarization sensitivity. In general, the polarization factors of the two instruments agree with each

other. For both instruments, band 8 has the largest polarization factor, about 0.04. The factors are smaller than 0.02 for all other bands except for Terra band 9 and for Aqua bands 18–19. For Terra band 9 and Aqua bands 18–19, the factors are about 0.028 and 0.027, respectively. These polarization measurements are all prelaunch, and there is considerable evidence that the polarization sensitivity of both sensors has changed since launch.

APPENDIX A
POLARIZATION EFFECT

The 2-D Hermitian matrix in (7) can always be expressed as

$$\mathbf{M} = \mathbf{M}_1 + i\mathbf{M}_2 \tag{A1}$$

where $\mathbf{M}_1$ and $\mathbf{M}_2$ are real 2-D symmetric and antisymmetric matrices, respectively. Then, (6) can be rewritten as

$$I' = \mathbf{E}^\dagger \mathbf{M}_1 \mathbf{E} + i\mathbf{E}^\dagger \mathbf{M}_2 \mathbf{E}. \tag{A2}$$

For a linear-polarized light

$$\mathbf{E} = \begin{pmatrix} \cos(\alpha) \\ \sin(\alpha) \end{pmatrix} E \tag{A3}$$

it is easy to see that $\mathbf{E}^\dagger \mathbf{M_2} \mathbf{E}$ is a real number. Then, we have

$$\begin{aligned} \mathbf{E}^\dagger \mathbf{M_2} \mathbf{E} &= \left(\mathbf{E}^\dagger \mathbf{M_2} \mathbf{E}\right)^\dagger \\ &= \mathbf{E}^\dagger \mathbf{M}_2^\dagger \mathbf{E} \\ &= -\mathbf{E}^\dagger \mathbf{M}_2 \mathbf{E}. \end{aligned} \tag{A4}$$

This means that

$$\mathbf{E}^\dagger \mathbf{M_2} \mathbf{E} = 0. \tag{A5}$$

Substituting (A5) into (A2), we get

$$I' = \mathbf{E}^\dagger \mathbf{M}_1 \mathbf{E}. \tag{A6}$$

Since $\mathbf{M}_1$ is a real symmetric matrix, we can always find a rotation matrix

$$\mathbf{T} = \begin{pmatrix} \cos(\delta) & -\sin(\delta) \\ \sin(\delta) & \cos(\delta) \end{pmatrix} \tag{A7}$$

where δ describes the transformation among the two components by the optical system, such that

$$\mathbf{M}_1 = \widetilde{\mathbf{T}} \begin{pmatrix} \lambda_1 & 0 \\ 0 & \lambda_2 \end{pmatrix} \mathbf{T}. \tag{A8}$$

Here, $\widetilde{\mathbf{T}}$ is the transpose of $\mathbf{T}$, λ_1, and λ_2 are eigenvalues of $\mathbf{M}_1$, and the two columns in $\mathbf{T}$ are corresponding eigenvectors of the matrix. Equation (A8) can be further expressed as

$$\begin{aligned} \mathbf{M}_1 &= \frac{\lambda_1 + \lambda_2}{2} \begin{pmatrix} 1 & 0 \\ 0 & 1 \end{pmatrix} + \frac{\lambda_1 - \lambda_2}{2} \widetilde{\mathbf{T}} \begin{pmatrix} 1 & 0 \\ 0 & -1 \end{pmatrix} \mathbf{T} \\ &= h \left[\begin{pmatrix} 1 & 0 \\ 0 & 1 \end{pmatrix} + a \begin{pmatrix} \cos(2\delta) & -\sin(2\delta) \\ -\sin(2\delta) & -\cos(2\delta) \end{pmatrix} \right] \end{aligned} \tag{A9}$$

where

$$h = \frac{\lambda_1 + \lambda_2}{2} \tag{A10}$$

is the averaged transmittance of the optical system and

$$a = \frac{\lambda_1 - \lambda_2}{\lambda_1 + \lambda_2} \tag{A11}$$

describes the polarization property of the optical system. Substituting (A3) and (A9) into (A6), we get

$$\begin{aligned} I' &= hE^\dagger E \left\{1 + a \left[\cos(2\delta)\left(\cos^2(\alpha) - \sin^2(\alpha)\right) \right.\right. \\ &\qquad \left.\left. - 2\sin(2\delta)\cos(\alpha)\sin(\alpha)\right]\right\} \\ &= hI \left\{1 + a\left[\cos(2\delta)\cos(2\alpha) - \sin(2\delta)\sin(2\alpha)\right]\right\} \\ &= hI \left\{1 + a\cos\left[2(\alpha + \delta)\right]\right\}. \end{aligned} \tag{A12}$$

APPENDIX B
RETRO-REFLECTED LIGHT EFFECT

Equation (22) can be rewritten as

$$\begin{aligned} w(\alpha) &= \left[1 + \nu_{11}\cos^2(\alpha) + (\nu_{12} + \nu_{21}) \right. \\ &\qquad \left. \times \cos(\alpha)\sin(\alpha) + \nu_{22}\sin^2(\alpha)\right]^2 \\ &= \left[1 + (\nu_{11} + \nu_{22})/2 + (\nu_{11} - \nu_{22})\cos(2\alpha)/2 \right. \\ &\qquad \left. + (\nu_{12} + \nu_{21})\sin(2\alpha)/2\right]^2 \end{aligned} \tag{B1}$$

where ν_{11}, ν_{12}, ν_{21}, and ν_{22} are the elements of $\mathbf{V}$. Let

$$\begin{aligned} q_0 &= 1 + (\nu_{11} + \nu_{22})/2 \\ q_1 &= (\nu_{11} - \nu_{22})/2 \\ q_2 &= (\nu_{12} + \nu_{21})/2. \end{aligned} \tag{B2}$$

Then, (B1) can be expressed as

$$\begin{aligned} w(\alpha) &= \left(q_0 + q_1\cos(2\alpha) + q_2\sin(2\alpha)\right)^2 \\ &= q_0^2 + q_1^2\cos^2(2\alpha) + q_2^2\sin^2(2\alpha) \\ &\quad + 2q_0q_1\cos(2\alpha) + 2q_0q_2\sin(2\alpha) \\ &\quad + 2q_1q_2\cos(2\alpha)\sin(2\alpha) \\ &= q_0^2 + q_1^2/2 + q_2^2/2 + (q_1^2 - q_2^2)\cos(4\alpha)/2 \\ &\quad + q_1q_2\sin(4\alpha) + 2q_0q_1\cos(2\alpha) + 2q_0q_2\sin(2\alpha). \end{aligned} \tag{B3}$$

From (B3), we can always determine a set of parameters, b_0, b_1, τ_1, b_2, and τ_2, and rewrite $w(\alpha)$ as

$$w(\alpha) = b_0\left\{1 + b_1\cos\left[2(\alpha + \tau_1)\right] + b_2\cos\left[4(\alpha + \tau_2)\right]\right\}. \tag{B4}$$

ACKNOWLEDGMENT

The authors would like to thank the MODIS developers at Raytheon/SBRS in Goleta, CA, particularly R. Drake and

J. Young for the continuing support of personnel. They would also like to thank S. Xiong, X. Wang, and S.-Y. Qiu for their contributions to this analysis, B. Wenny for his valuable comments, and E. Waluschka for helpful comments, particularly for helpful discussions and suggestions.

REFERENCES

[1] W. L. Barnes and V. V. Salomonson, "MODIS: A global image spectroradiometer for the Earth Observing System," *Critical Rev. Opt. Sci. Technol.*, vol. CR47, pp. 285–307, 1993.

[2] W. L. Barnes, T. S. Pagano, and V. V. Salomonson, "Prelaunch characteristics of the Moderate Resolution Imaging Spectroradiometer (MODIS) on EOS-AM1," *IEEE Trans. Geosci. Remote Sens.*, vol. 36, no. 4, pp. 1088–1100, Jul. 1998.

[3] W. L. Barnes, V. V. Salomonson, B. Guenther, and X. Xiong, "Development, characterization, and performance of the EOS MODIS sensors," in *Proc. SPIE—Earth Observing Systems VIII*, 2003, vol. 5151, pp. 337–345.

[4] W. L. Barnes, X. Xiong, and V. V. Salomonson, "Status of Terra MODIS and Aqua MODIS," *J. Adv. Space Res.*, vol. 32, no. 11, pp. 2099–2106, 2003.

[5] C. O. Justice, E. Vermote, J. R. G. Townshend, R. Defries, D. P. Roy, D. K. Hall, V. V. Salomonson, J. L. Privette, G. Riggs, A. Strahler, W. Lucht, R. B. Myneni, P. Lewis, and M. J. Barnsley, "The Moderate Resolution Imaging Spectroradiometer (MODIS): Land remote sensing for global change research," *IEEE Trans. Geosci. Remote Sens.*, vol. 36, no. 4, pp. 1228–1249, Jul. 1998.

[6] W. E. Esaias, M. R. Abbott, I. Barton, O. W. Brown, J. W. Campbell, K. L. Carder, D. K. Clark, R. L. Evans, F. E. Hoge, H. R. Gordon, W. P. Balch, R. Letelier, and P. J. Minnett, "An overview of MODIS capabilities for ocean science observations," *IEEE Trans. Geosci. Remote Sens.*, vol. 36, no. 4, pp. 1250–1265, Jul. 1998.

[7] M. D. King, W. P. Menzel, Y. J. Kaufman, D. Tanre, B. C. Gao, S. Platnick, S. A. Ackerman, L. A. Remer, R. Pincus, and P. A. Hubanks, "Cloud and aerosol properties, precipitable water, and profiles of temperature and water vapor from MODIS," *IEEE Trans. Geosci. Remote Sens.*, vol. 41, no. 2, pp. 442–458, Feb. 2003.

[8] C. L. Parkinson, "Aqua: An Earth-Observing Satellite mission to examine water and other climate variables," *IEEE Trans. Geosci. Remote Sens.*, vol. 41, no. 2, pp. 173–183, Feb. 2003.

[9] X. Xiong and W. L. Barnes, "An overview of MODIS radiometric calibration and characterization," *Adv. Atmos. Sci.*, vol. 23, no. 1, pp. 69–79, 2006.

[10] X. Xiong, K. Chiang, J. Esposito, B. Guenther, and W. Barnes, "MODIS on-orbit calibration and characterization," *Metrologia*, vol. 40, no. 1, pp. S89–S92, Feb. 2003.

[11] X. Xiong, J. Sun, J. Esposito, B. Guenther, and W. L. Barnes, "MODIS reflective solar bands calibration algorithm and on-orbit performance," in *Proc. SPIE—Optical Remote Sensing of the Atmosphere and Clouds III*, 2003, vol. 4891, pp. 95–104.

[12] J. Sun, X. Xiong, B. Guenther, and W. Barnes, "Radiometric stability monitoring of the MODIS reflective solar bands using the moon," *Metrologia*, vol. 40, no. 1, pp. S85–S88, 2003.

[13] X. Xiong, N. Che, and W. Barnes, "Terra MODIS on-orbit spatial characterization and performance," *IEEE Trans. Geosci. Remote Sens.*, vol. 43, no. 2, pp. 355–365, Feb. 2005.

[14] G. W. Kattawar, G. N. Plass, and J. A. Guinn, "Monte Carlo calculations of the polarization of radiation in the Earth's atmosphere–ocean system," *J. Phys. Oceanogr.*, vol. 3, no. 4, pp. 353–372, Oct. 1973.

[15] A. Ivanoff, "Polarization measurements in the sea," in *Optical Aspects of Oceanography*, N. G. Jerlov and E. S. Nielsen, Eds. London, U.K.: Academic, 1974, pp. 151–175.

[16] J. B. Young, E. Knight, and C. Merrow, "MODIS polarization performance and anomalous four-cycle polarization phenomenon," *Proc. SPIE*, vol. 3439, pp. 247–256, 1998.

[17] R. C. Levy, L. A. Remer, and Y. J. Kaufman, "Effects of neglecting polarization on the MODIS aerosol retrieval over land," *IEEE Trans. Geosci. Remote Sens.*, vol. 42, no. 11, pp. 2576–2583, Nov. 2004.

[18] G. Meister, E. J. Kwiatkowska, B. A. Franz, F. S. Patt, G. C. Feldman, and C. R. McClain, "Moderate-Resolution Image Spectroradiometer ocean color polarization correction," *Appl. Opt.*, vol. 44, no. 26, pp. 5524–5535, Sep. 2005.

[19] M. Pavlov, *Polarization Insensitivity, Test Procedure for (ALPC-08)*. Goleta, CA: Santa Barbara Research Center, Mar. 24, 1996.

[20] J. Sun, J. Xiong, X. Wang, S. Qiu, S. Xiong, and E. Waluschka, "Results and lessons learned from MODIS polarization sensitivity characterization," *Proc. SPIE*, vol. 6296, pp. 629 605-1–629 605-10, 2006.

[21] N. Souaidia, D. Moyer, G. Meiser, S. Pellicori, E. Waluschka, and K. Voss, "MODIS polarization ray tracing analysis," *Proc. SPIE*, vol. 5888, pp. 140–147, 2005.

[22] E. Waluschka, "MODIS polarization measurements and simulation and the 4θ effect," *Proc. SPIE*, vol. 3121, pp. 278–287, 1997.

[23] S. Huard, *Polarization of Light*. Chichester, U.K.: Wiley, 1997.

Jun-Qiang Sun received the B.S. degree in physics from Changsha Institute of Technology, Changsha, China, the Ph.D. degree in physics from the University of Science and Technology of China, Hefei, and the Ph.D. degree in chemistry from the University of Florida, Gainesville.

He has worked in the fields of atomic and molecular physics at Freie Universitaet Berlin and the University of Kansas and in quantum chemistry at Iowa State University and the University of Florida. He has worked with the MODIS Calibration Support Team for more than seven years. He is currently a Senior Scientist with Science Systems and Applications, Inc., Lanham, MD, where he currently works on The Visible Infrared Imager/Radiometer Suite (VIIRS) instrument calibration and characterization. He has published more than 35 journal papers in physics, chemistry, and remote-sensor calibration.

Xiaoxiong Xiong received the B.S. degree in optical engineering from the Beijing Institute of Technology, Beijing, China, and the Ph.D. degree in physics from the University of Maryland, College Park.

He has worked in the fields of optical instrumentation, nonlinear optics, laser/atomic spectroscopy, and mass spectrometry at private industry and at the National Institute of Standards and Technology. He is currently an Optical Physicist at the NASA Goddard Space Flight Center, Greenbelt, MD, working on the Earth Observing System and NPOESS Preparatory Project (NPP) sensor calibration and characterization. He is currently serving as the MODIS Project Scientist for instrument operation and calibration and the Technical Lead for both the MODIS Characterization Support Team and the NPP Instrument Calibration Support Team.